SLAT NOISE ASSESSMENT FROM A340 FLYOVER ACOUSTIC MEASUREMENTS WITH A MICROPHONE PHASED ARRAY 4$^{\text{TH}}$ BERLIN BEAMFORMING CONFERENCE

Vincent Fleury and Patrice Malbéqui*

Onera

29 avenue de la Division Leclerc, 92322 Châtillon, France.

ABSTRACT

To predict and optimize the noise impact of aircraft traffic around airports, airframe noise needs to be described by simple but reliable acoustic models. Semi-empirical and analytical models for high-lift and landing-gear noise are found in the literature for instance. The present work is focused on the assessment of slat noise from real aircraft flyover noise measurements. The aircraft is an Airbus A340 during approach. The originality of the approach is that it uses a recent beamforming-based deconvolution technique. The main interest of the method is to spatially separate the various airframe noise sources and to provide their individual de-Dopplerized acoustic levels over a range of more than 10 dB. Slat noise spectra and directivity patterns are computed for two flight velocities, 150 kts and 175 kts. The obtained results are in good agreement with the prediction from the slat noise model of Dobrzynski & Pott-Pollenske [AIAA paper 2001-2158]. Beamforming-based deconvolution techniques prove to be efficient tools to analyze real aircraft flyover noise.

1 INTRODUCTION

The prediction of noise impact due to air traffic around airports is very challenging. Since comprehensive and accurate computational approaches are currently not viable, simple but realistic prediction tools are required. For instance, in the IESTA global evaluation platform developed by Onera[17] (IESTA: Infrastructure for Evaluating Air Transport Systems), airframe noise is evaluated from semi-empirical and analytical acoustic source models and the propagation effects are derived from pre-computed numerical simulation

---

*Department of Computational Fluid Dynamics and Aeroacoustics (DSNA)

results. A similar approach is adopted in the PANAM platform of DLR[4] and in the ANOPP2 program of NASA[16].

Acoustic models of most of the airframe noise sources, involving high-lift devices and landing-gears, are found in the literature. They are established from dedicated aeroacoustic wind-tunnel tests or from theoretical approaches. Concerning slat noise, Molin *et al.*[18] and Molin & Roger[19] use the Amiet's theory[1] to predict the noise contribution due to pressure fluctuations along slats and slat-horn devices, respectively. From the large database collected in the DLR's AWB and the DNW's LFF facilities, Dobrzynski & Pott-Pollenske[8] have built a semi-empirical slat noise model too. For flap noise, a trailing edge acoustic model was developed by Howe[15] and a side-edge noise model by Howe[14] and Brooks[5]. A semi-empirical approach of flap noise is also found in Ref. [10]. Landing gear noise is addressed by Dobrzynski[7, 21] both from reduced and full-scale wind-tunnel tests.

Currently, to assess these prediction tools from real flyover noise tests, the procedure consists of performing two successive flyovers, one with the tested device deployed and another one in clean configuration. The influence of the tested device is then obtained by subtracting acoustic spectra. However, when the device under investigation is not the dominant noise source, the result may be poorly reliable. Furthermore, the flight conditions of both flyovers need to be similar (except for the tested device), which is sometimes impossible to obtain from flight mechanics considerations. With the recent development of beamforming-based deconvolution techniques for moving sources, more accurate and robust analyses of flyover noise data can be obtained. Indeed, due to the high signal-to-noise ratio of beamforming procedures, acoustic sources of very different noise ranges (more than 10 dB difference) can be determined from a single flyover noise dataset. Several examples of applications are found in the literature, see Refs.[6, 12, 22, 23] for instance.

The present paper is focused on slat noise. The main interest of this work is to use a recent beamforming-based deconvolution technique to provide a detailed comparison of real aircraft flyover noise measurements and slat noise prediction models. The aircraft is an Airbus A340-300 with CFM56-5C2 engines during approach. The dataset has been obtained within the European program AWIATOR. The test matrix and the experimental setup are described in Sec. 2. The beamforming and deconvolution algorithms are presented in Sec. 3. The resulting acoustic maps, slat noise narrow-band spectra and overall directivity patterns are shown in Sec. 4. The results are compared to prediction models in Sec. 4 too.

2 EXPERIMENTS

The test campaign was carried-out at Tarbes, France, in 2006. The aircraft is flown by Airbus and the microphone phased-array measurements are performed by Onera.

2.1 Test conditions

The aircraft follows a conventional approach trajectory. The slat and flap deflection angles are 23° and 32°, respectively. Moreover, the landing-gears are up and the engines

are at only 30% rating. Two flight velocities are considered, 150 kts and 175 kts. Flight characteristics along with meteorological conditions are provided in Table 1. The aircraft trajectory is provided by Airbus with a DGPS system.

One of the objectives of the AWIATOR program is to test the aerodynamic performance of innovative Trailing Edge Devices (TED) on the flaps. For the present study, only flyovers with zero TED deflection angles are analyzed. It is therefore thought that these devices have a limited influence on slat noise. Indeed, from Ref.[8] the impact of the flaps on slat noise mostly concerns the overall noise level (by introducing a constant gain, in dB scale) and a cut-off Strouhal number. This is specified in the discussion of slat noise spectra in Sec. 4.2.

conf.	M_{flight}	H (m)	descending angle (°)	P (hPa)	T (deg. K)	H_r (%)	wind speed (m/s)	cross wind speed (m/s)
#150	0.23	168	4.3	0.981	294	44	2.4	0.8
#175	0.26	158	3.3	0.981	293	56	4.3	3.1

Table 1: Flight and meteorological conditions. M_{flight} is the flight Mach number, H is the altitude at the emission angle $\Theta = 90°$ (see Figure 4) and P, T and H_r are the atmospheric pressure, temperature and relative humidity at 10 m above the ground, respectively.

2.2 Measurement setup

Microphone array

A cross-shaped array with 121 microphones is used, see Figure 1. The overall arrangement can be subdivided into 11 sub-arrays, see Figure 2. The sub-arrays are designed so that the beamformer output has similar performances for each third-octave band between 500 Hz and 5 kHz (11 third-octaves). More precisely, (i) a space resolution of 4 m is required when the acoustic source is at $H = 150$ m altitude and $\theta = 90°$ emission angle and (ii) for each possible acoustic source over the airframe, no aliased image must be located on the airframe. The size of the sub-arrays is determined from the condition (i) and the (uniform) interval between the microphones is dictated by (ii). The overall arrangement of the microphone array is also designed in order to minimize the total number of necessary microphones, see Figure 2. From Table 1, the actual flight height H is close to the prescription $H = 150$ m. Thus, the conditions (i) and (ii) are truly satisfied. Actually, the investigated frequency axis ranges from 100 Hz to 5 kHz, every $\Delta f = 50$ Hz. For the frequencies lower than 500 Hz, the condition (i) is then not valid (but (ii) is satisfied). In this case, the deconvolution procedure, see Sec. 3.2, is still expected to provide a satisfying space resolution.

The microphones are 4135 1/4' B&K microphones. They are mounted on rigid (epoxy) 50-cm-spanwise plates, see Figure 1. The plates are supported by 2 long wire cables at roughly 30 cm above the ground.

Acquisition

A 24-bites commercial system (LMS, SCADAS 3) is used to acquire the 121 microphone signals. The so-called top and time GPS signals (2 channels) are also acquired in order to synchronize the measurements and the aircraft trajectory provided by Airbus. The acquisition is performed at $f_e = 51.2$ kHz sampling frequency, over 20 s length. The reason for choosing such a high acquisition frequency, much higher than twice the highest frequency under study ($2 \times 5000 \times 2^{1/6} \approx 11$ kHz), is given in Sec. 3.1.
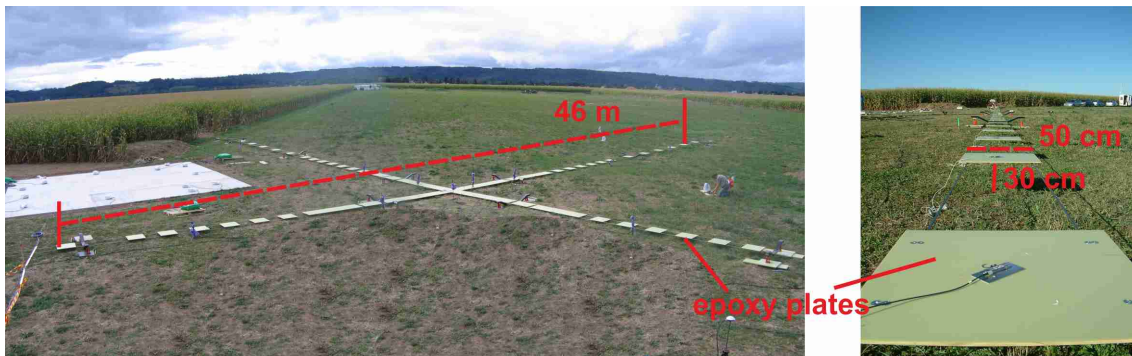
Figure 1: Cross-shaped microphone array.
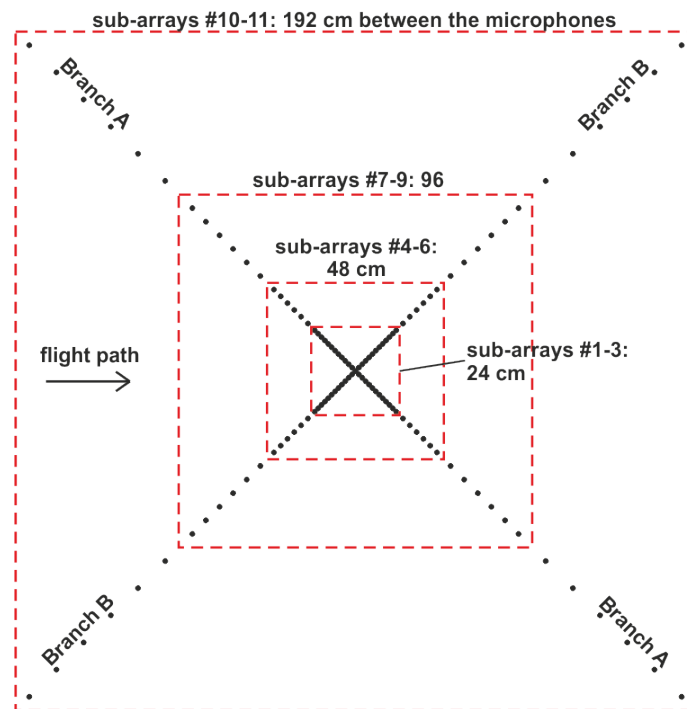
Figure 2: Sketch of the microphone array.

3 DATA ANALYSIS

The noise sources are sought over a source domain that closely follows the airframe sil-
houette and the dihedral angle of the wings (not shown), see Figure 3. This domain is
sampled by $N_S = 4066$ source points with a resolution of roughly 80 cm. The acoustic
level emitted from the source points is estimated in two stages. First, the microphone
phased-array data are analyzed by a beamforming procedure. A deconvolution technique
is then used to remove the so-called *point spread function* from the beamformer output.
The analysis is carried-out for specific emission angles, from $\theta = 50°$ to $\theta = 130°$ every
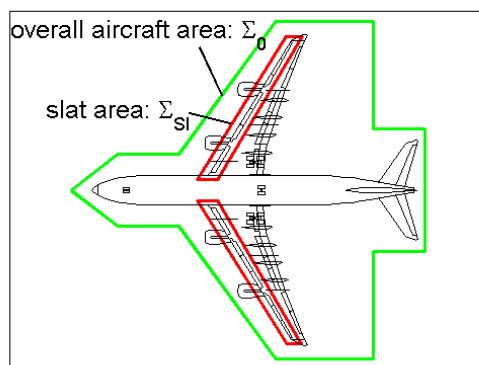20°, see Figure 4. The two stages of the procedure are detailed in the next sections.

Figure 3: *Definition of the overall aircraft area (green) and of the slat area (red). The
source domain follows the dihedral angle of the wings in order to reduce parallax
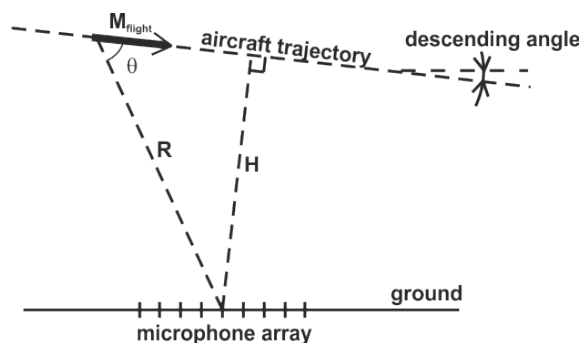issues (not shown).*

Figure 4: *Emission angle θ and characteristic source-to-microphone distances R and H.*

3.1 Beamforming acoustic maps

The first stage uses the *beamforming-MS* methodology detailed in Ref. [11]. The task relies on the computation of the following expressions

$$b_i = \frac{1}{N_K} \sum_{k=1}^{N_K} \sum_{(m,n) \in S} G_{i,m}^{(k)*} w_m \frac{\hat{p}_{i,m}^{(k)}}{\alpha_{i,m}^{(k)}} \frac{\hat{p}_{i,n}^{(k)*}}{\alpha_{i,n}^{(k)}} w_n G_{i,n}^{(k)} \qquad (1)$$

and

$$H_{i,j} = \frac{1}{N_K} \sum_{k=1}^{N_K} \sum_{(m,n) \in S} G_{i,m}^{(k)*} w_m G_{j,m}^{(k)} G_{j,n}^{(k)*} w_n G_{i,n}^{(k)}. \qquad (2)$$

The beamforming acoustic map is then obtained by allocating the acoustic level

$$s_i^{\text{beam.}} = \frac{b_i}{H_{i,i}}$$

to every source points, $i = 1$ to $i = N_S$. The remainder of this section is devoted to define all the quantities involved in Eqs. (1) and (2) and to comment these equations.

Let t_0 be the emission time corresponding to the emission angle θ under study. The emission time axis is then uniformly subdivided into N_K time blocks around t_0. For instance, the kth time block is centered around the emission time

$$t_0^{(k)} = t_0 + \left(k - \frac{N_K - 1}{2} \right) \Delta_T. \qquad (3)$$

where $\Delta_T = 1/\Delta_f$ is the length of the blocks with Δ_f the required frequency resolution. As indicated in Ref. [11], the total displacement $D = N_K \Delta_T U_{\text{flight}}$ needs to be much lower than the characteristic source-to-microphone distance R, see Figure 4. With $\Delta_f = 50$ Hz and $N_K = 15$, $D = 23$ m ($D = 27$ m respectively) for the flight velocity $U_{\text{flight}} \approx 150$ kts ($U_{\text{flight}} \approx 175$ kts respectively), which is indeed much lower than $R = H \approx 168$ m at $\theta = 90°$ ($R = 158$ respectively), see Table 1.

Moreover, $G_{i,m}^{(k)}$, $G_{j,m}^{(k)}$, $G_{i,n}^{(k)}$ and $G_{j,n}^{(k)}$ in Eqs. (1) and (2) represent the frequency-domain Green functions between the source points, i and j, and the microphones, m and n. They also correspond to the emission time $t_0^{(k)}$, see Eq. (3). For instance

$$G_{i,m}^{(k)} = \frac{1}{R_{i,m}^{(k)}} \exp \left(\frac{\tilde{\imath} 2\pi f R_{i,m}^{(k)}}{c \left(1 - M_{i,m}^{(k)} \right)} \right), \qquad (4)$$

where $R_{i,m}^{(k)}$ and $M_{i,m}^{(k)}$ are the distance and the projected Mach number, respectively, between i and m at the emission time $t_0^{(k)}$. Furthermore, in Eq. (4) f is the frequency, c is the sound speed and $\tilde{\imath}$ is the imaginary unit ($\tilde{\imath}^2 = -1$). Contrary to Ref. [11], the Doppler amplification factor is not included in Eq. (4). Indeed, the required Doppler amplification factor depends on the type of noise sources. The acoustic efficiency of a

moving monopole is $1/(1 - M_{i,m})$, $1/(1 - M_{i,m})^2$ for a dipole, *etc.* Since we do not know *a priori* the type of noise sources to be dealt with, no correction is applied. Instead, the modification of the acoustic level due to the projected Mach number between the noise sources and the microphones is implicitly attributed to the acoustic level emitted by the sources. The comparison of the present flyover slat noise results with static models (from wind tunnel measurements) should consequently be performed by incorporating flyover effects into the wind-tunnel-based predictions. This will be clarified in Sec. 4.2.

In Eq. (1), $\hat{p}_{i,m}^{(k)}$ (similarly for $\hat{p}_{i,n}^{(k)}$) is the complex Fourier component of the microphone signal $p_m(t)$ for the Doppler frequency $f/(1 - M_{i,m}^{(k)})$. An energy-preserving Hanning window function is used to reduce frequency-domain side-lobes. Furthermore, the computation is performed over a time interval $T_{i,m}^{(k)}$ centered around the reception time $t_0^{(k)} + R_{i,m}^{(k)}/c$. Its length is $\Delta_T(1 - M_{i,m}^{(k)})$ and it has $N_t = f_e/\Delta_f$ samples. Since these time samples generally do not coincide with the acquisition times over $T_{\text{ac.}}$, the microphone data need to be interpolated from $T_{\text{ac.}}$ to $T_{i,m}^{(k)}$. A simple cubic spline interpolation scheme is applied. In order to limit the modification of signal due to interpolation, the acquisition frequency f_e must be much higher than the studied frequency $f/(1 - M_{i,m}^{(k)})$, see Ref. [20]. In the present case, $f_e = 51.2$ kHz is around 10 times higher than the maximal reception frequency, which is enough for a cubic spline interpolation scheme.

Following the conclusions of Ref.[9] concerning cross-shaped microphone arrays, the set of microphone indexes $(m, n) \in S$ in Eqs. (1) and (2) is decomposed as $S = (S_A, S_B)$, where S_A refers to microphones over the A microphone branch, see Figure 2, and S_B to the B branch. As explained in Sec. 2.2, the microphone array is sub-divided into 11 sub-arrays that need to be chosen in function of frequency. The size of these sub-arrays L_0 has be determined for the emission angle $\theta = 90°$ only. However, the resolving power of beamforming Δ_X also depends on the emission angle θ and on the flight Mach number M_{flight}. Indeed, Δ_X is proportional to $\lambda_{\text{Dop.}}R/(L\sin\theta)$ where $\lambda_{\text{Dop.}} = c/f_{\text{Dop.}}$ is the acoustic wave length for the Doppler frequency $f_{\text{Dop.}} = f/(1 - M_{flight}\cos\theta)$. Thus, in order to obtain a constant space resolution Δ_X in function of θ and M_{flight}, the length L of the sub-arrays S_A and S_B must adapted as follows

$$L = L_0(f)\frac{1 - M_{\text{flight}}\cos\theta}{\sin^2\theta}. \tag{5}$$

In practice, for each frequency f and emission angle θ, S_A and S_B are determined by adding or removing a few microphones within the initially designed sub-array in order to satisfy to Eq. (5) as closely as possible.

In Eqs. (1) and (2), the weighting terms w_m and w_n represent the Hanning window function over the microphone sub-arrays $m \in S_A$ and $n \in S_B$, respectively. Furthermore, $\alpha_{i,m}^{(k)}$ and $\alpha_{i,n}^{(k)}$ in Eq. (1) are used to compensate the acoustic attenuation due to atmospheric effects. Their expression (in dB<0) is of the form

$$\alpha_{i,q}^{(k)} = \alpha\left(\frac{f}{1 - M_{i,q}^{(k)}}, P, T, H_r\right) R_{i,q}^{(k)}, \quad \text{(dB)}$$

for $q = m$ or $q = n$. The α function (in dB/m) is tabulated in Refs. [2, 3]. The

atmospheric pressure P, temperature T and relative humidity H_r are given in Table 1 for each flyover.

3.2 Deconvolution and acoustic levels

In order to estimate noise source levels, the beamformer output Eq. (1) needs to be deconvolved. The *DAMAS-MS* methodology is followed, see Ref. [11]. The problem to be solved writes

$$\boldsymbol{Hs} = \boldsymbol{b} + \kappa^2 \Delta \boldsymbol{s} \tag{6}$$

with the positivity constraint $s_i \geq 0$, for all $i = 1, ...N_S$. The $N_S \times N_S$ matrix $\boldsymbol{H}$ and the $N_S \times 1$ vector $\boldsymbol{b}$ are defined in Eqs. (2) and (1), respectively. The second term of the right-hand side of Eq. (6) is introduced to control the deconvolution process. It is based on the 2D-cartesian Laplacian of the solution $\boldsymbol{s}$. Its strength is determined by the regularization parameter κ. The problem defined by Eq. (6) along with the positivity condition are solved with a conventional constraint iterative fixed-point procedure, see Ref. [11].

To choose the appropriate regularization parameter κ is actually a crucial task. When κ is too small, the iterative deconvolution procedure may not converge, see Figure 5(a) for illustration. When κ is too large, the regularization term Δs leads to very smooth acoustic maps (not shown). From the results of Figure 5(a) and 5(b), a solution-*vs.*-residue curve is plotted in Figure 5(c) as function of κ. The application of the L-curve criterium of Hansen[13] then enables us to determine the optimal regularization parameter. In the present example, the optimum is between $\kappa = 10^{-3}$ and $\kappa = 10^{-2}$ (but closer to 10^{-3}). Figure 5(d) also shows that the number of iterations required to get the convergence of the total acoustic level $\|s\|_1$ increases with κ. It is therefore preferable to take a small value of κ for computational cost issues. Furthermore, $\|s\|_1$ is roughly the same between $\kappa = 10^{-3}$ and $\kappa = 10^{-2}$. In the remainder, the slightly sub-optimal value $\kappa = 10^{-3}$ is chosen. Due to the heavy computational cost required to apply the L-criterium, the same value of the regularization parameter $\kappa = 10^{-3}$ is used for the whole frequencies, emission angles θ and the two flyovers. Moreover, the number of iterations is limited to 4000. The good convergence of the deconvolution process is checked for every cases (different frequencies, emission angles and flyovers).

Slat noise is finally evaluated by simply summing-up all the deconvolved source levels s_i over the slat area, see Figure 3,

$$S_{\text{Sl}}(f, \theta) = \sum_{i \in \Sigma_{\text{Sl}}} s_i(f, \theta). \tag{7}$$

As shown in Figure 3, the engine nozzle exits are included in the chosen slat area. In the present flight configurations the engines are in idle and it is therefore assumed that engine noise is much less intense than slat noise. This is the reason why the slat noise area encompasses the engine exhausts.
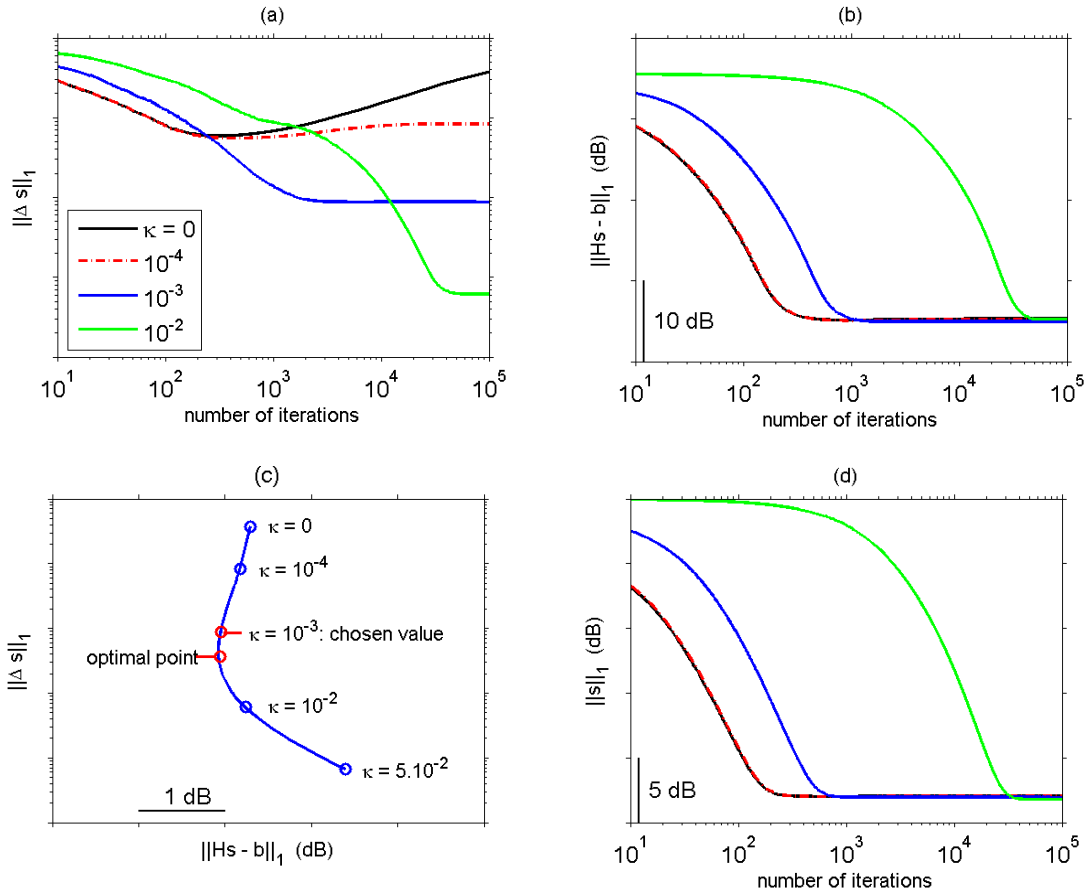
Figure 5: Example of convergence curves for the #150 flight configuration at 1 kHz and
θ = 90°. In (c), as many as 10^6 iterations are needed to get the convergence of
$\|\Delta s\|_1$ and $\|Hs - b\|_1$ for $\kappa = 5 \cdot 10^{-2}$, and 10^5 iterations for $\kappa \leq 10^{-2}$.

4 RESULTS

4.1 Acoustic maps

The benefit of deconvolution is shown by the example seen in Figure 6. Specifically, the space resolution of the deconvolved acoustic maps is much better than on the beamforming source maps. A few parasitic sources, especially downstream of the wings, are still not removed by the DAMAS-MS procedure. This can be due to both statistical convergence issues (only $N_K = 15$ data blocks are used to compute the acoustic maps) and to sidelobes from strong noise sources of different frequencies. Indeed, the problem of moving noise source level estimation basically involves all the sources over the whole frequency domain. To separate the sources according to frequency as in Eq. (6) for instance, the conventional Doppler frequency assumption needs to be introduced, which is an approximation. Thus, the estimated solutions can be partially coupled between different frequencies, see Ref. [11] for further details. The imperfect symmetry of the noise source levels over the airframe is also attributed to the poor statistical convergence of noise data on the one hand, and to the unavoidable uncertainties of real aircraft noise sources on the other hand. In the next section, the present integrated slat noise source levels are assessed from straightforward acoustic measurements.
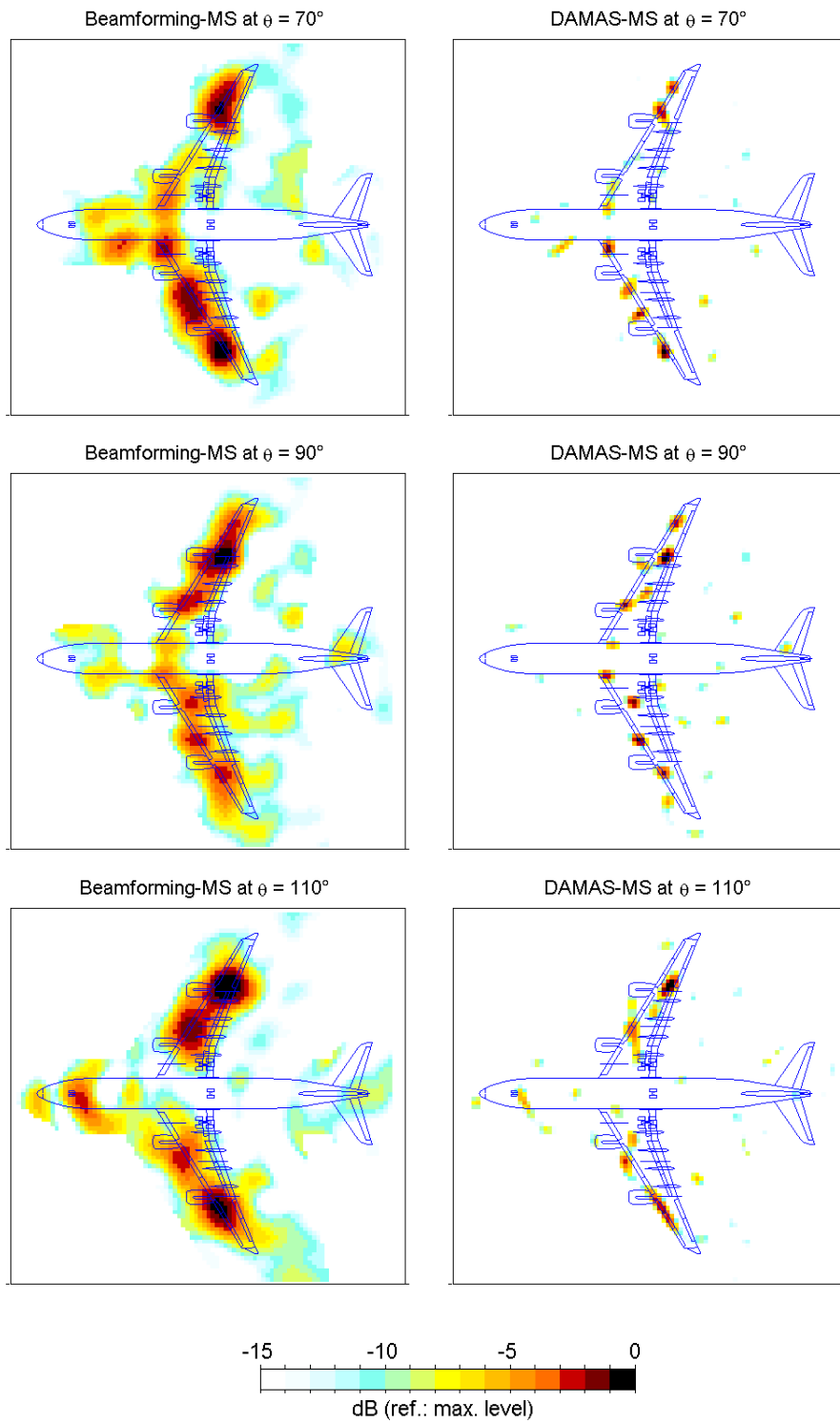
Figure 6: Beamforming (left) and deconvolved (right) acoustic maps at 800 Hz (narrow-band) for the flyover #150. Three emission angles are considered, $\theta = 70°$, $90°$ and $110°$.

4.2 Acoustic levels

Validation

In order to quantitatively validate the results, the deconvolved acoustic source levels are integrated over the entire airframe area (Σ_0 in Figure 3) and then extrapolated to the ground in order to be compared to reference ground measurements. The extrapolation of the deconvolved noise levels s_i to the ground is performed as follows,

$$P^{\text{sources}\rightarrow\text{ground}}\left(\frac{f}{1-M_{i_0,m_0}},\theta\right) = \frac{\alpha_{i_0,m_0}^2}{R_{i_0,m_0}^2}\sum_{i\in\Sigma_0}s_i(f,\theta). \tag{8}$$

In Eq. (8) i_0 is the index of the source point in the middle of the airframe area and m_0 is the index of the center microphone. Furthermore, M_{i_0,m_0}, R_{i_0,m_0} and α_{i_0,m_0} are computed for the single emission time $t_0(\theta)$. The frequency resolution of $P^{\text{sources}\rightarrow\text{ground}}$ is $\frac{\Delta_f}{1-M_{i_0,m_0}}$ ($\Delta_f = 50$ Hz). Furthermore, the reference ground noise spectra are computed as follows,

$$P^{\text{ground}}(f_{\text{ground}},\theta) = \frac{1}{N_M N_K}\sum_{m=1}^{N_M}\sum_{k=1}^{N_K}\left|\hat{p}_m^{(k)}(f_{\text{ground}})\right|^2, \tag{9}$$

As previously, an energy-preserving Hanning window function is used with the computation of the Fourier transform of the microphone signal $p_m(t)$. Furthermore, k refers to a specific data block of length $\Delta_T = 0.02$ s amongst $N_K = 15$ samples. The data blocks are evenly distributed on both sides of the reception time $t_0 + R_{i_0,m_0}/c$ corresponding to the tested emission angle θ. The frequency resolution of P^{ground} is $\Delta_f = 50$ Hz.

Figure 7 (left), the extrapolated spectra $P^{\text{sources}\rightarrow\text{ground}}$ are compared to the reference spectra P^{ground} for several emission angles θ. The fairly good agreement of these results validates the computation of the deconvolved acoustic levels integrated over the entire airframe area Σ_0. The extrapolated overall directivity pattern is also compared to reference measurements in Figure 7 (right). A discrepancy by less than 1 dB is obtained, which is deemed negligible.

Slat noise

As indicated in Eq. (7), slat noise spectra are estimated by integrating the deconvolved acoustic levels over the slat area. The obtained spectra are plotted in Figure 8 (left) for several emission angles. In order to validate these results, the data are also plotted as function of the Strouhal number St_{CS} based on the mean slat chord and the flight velocity, see Figure 8 (right). From the conclusions of Dobrzynski and Pott-Pollenske[8], the present slat noise spectra should then follow the semi-empirical laws

$$\begin{aligned} S_{\text{Sl}} &\propto \text{St}^{0.3} &&\text{for } \text{St} < \text{St}_0,\\ S_{\text{Sl}} &\propto \text{St}^{-1.8} &&\text{for } \text{St} > \text{St}_0. \end{aligned} \tag{10}$$

By taking the cut-off Strouhal number St_0 around $\text{St}_0 = 4.5$, the agreement is indeed satisfying, at least for $\theta \leq 110°$. In Ref.[21], St_0 is rather 2.5 (see Figure 8 of Ref.[21]).
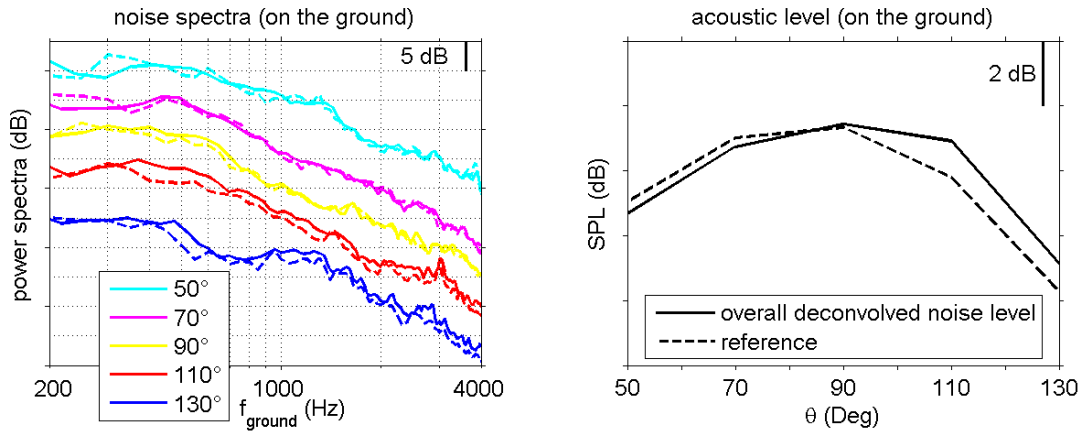
Figure 7: *The deconvoled noise levels integrated over the entire airframe area are extrapolated to the ground (plain lines, see Eq. (8)) and compared to straightforward ground measurements (dashed lines, see (Eq. 9)). The ground frequency axis f_{ground} is reduced to [200 Hz ; 4 kHz] in order to be common for all the emission angles θ. (left) For clarity reasons, the noise spectra are arbitrarily shifted in the y-coordinate direction from an emission angle to another one. (right) For each emission angle, the acoustic level is obtained by integrating the acoustic spectra from 200 Hz to 4 kHz.*

However, the cut-off Strouhal number depends on the slat and flap deflection angles, namely 23° and 32° in the present study, respectively. In Ref.[21], the deflection angles are rather 27° and 40°, which may explain the difference. Furthermore, the presence of TED devices modifies the flow circulation around the wing, which also has an influence on St_0. The agreement between the present slat noise spectra and the semi-empirical law Eq. (10) is satisfying, at least for $\theta \leq 110°$.

The de-Dopplerized slat noise spectra have been integrated from 100 Hz to 5 kHz (emission frequency). The result is shown in Figure 9 (left) for several emission angles θ. The two flight velocities are also considered, *i.e.* 150 kts and 175 kts. In order to use results from static tests in wind-tunnels for comparison, supplementary moving source effects need to be corrected in the present flyover noise data. Indeed, by assuming that the slat acoustic efficiency is dipolar, a $(1 - M \cos \theta)^{-4}$ amplification term needs to be corrected. Then, from Ref. [21] the following directivity pattern model is expected

$$D(\theta) \propto \sin^2(\theta - \delta_S) + 0.1 \cos^2(\theta - \delta_S), \tag{11}$$

where $\delta_S = 23°$ is the slat deflection angle. Furthermore, slat noise noise should follow a $M_{flight}^{4.5}$ power law, see Ref. [21] too. Figure 9 (right) is plotted in order to assess the present flyover slat noise data from this tabulated acoustic model. The comparison is in good agreement, which again shows the relevance of the obtained flyover slat noise levels.
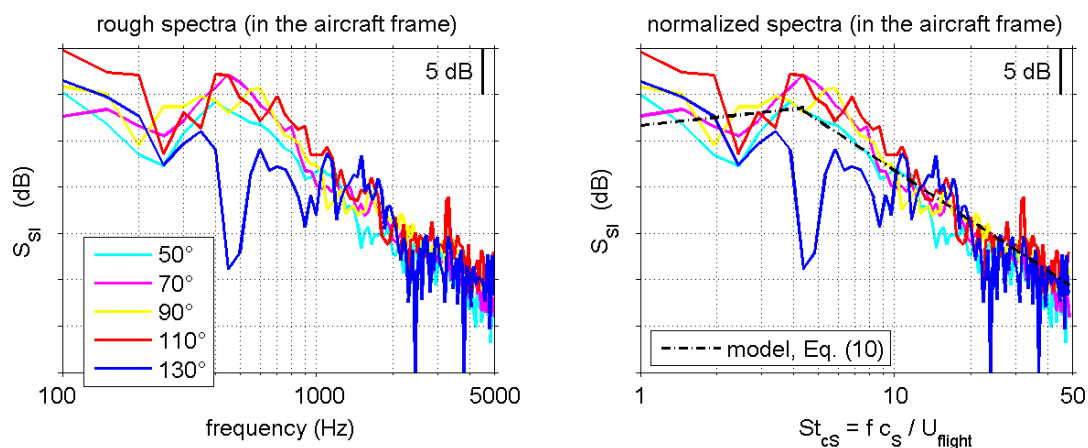
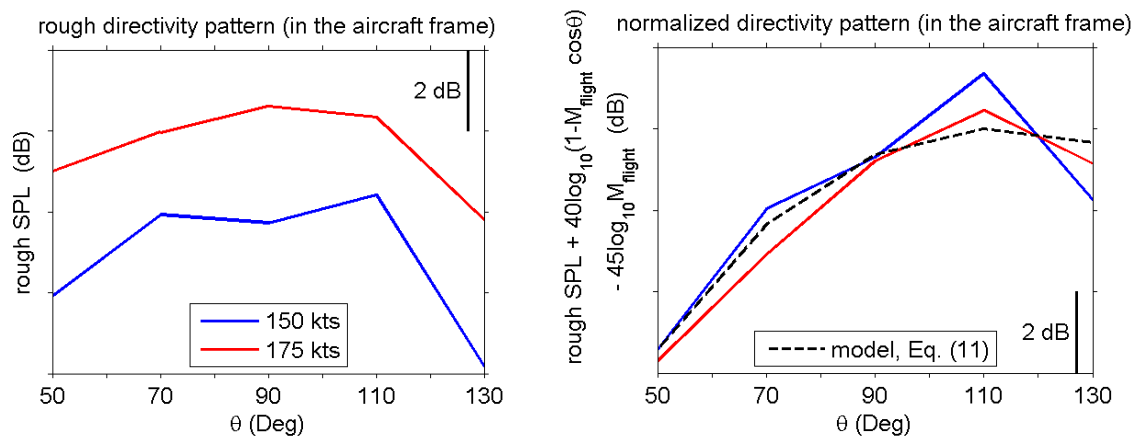*Figure 8: Slat noise spectra in the aircraft frame. Test case #150.*

Figure 9: Slat noise directivity patterns in the aircraft frame.

5 CONCLUSION

Slat noise has been evaluated from real A340 flyover noise data during approach. Two flight velocities have been studied, 150 kts and 175 kts. The acoustic measurements have been performed with a cross-shaped microphone array. The noise levels have been estimated by using a beamforming-based deconvolution technique, DAMAS-MS. The obtained de-Dopplerized slat noise levels (spectra and directivity pattern) have been compared to acoustic models found in the literature. These models are issued from static wind-tunnel tests. The fairly close agreement of these data validates the flyover slat noise results. The present approach could be used to analyze other airframe devices and noise reduction concepts from real aircraft noise measurements.

6 ACKNOWLEDGEMENT

References

[1] R. K. Amiet. "Acoustic Radiation from an Airfoil in a Turbulent Stream." *J. Sound and Vibration*, 41(4), 407–420, 1975.

[2] H. E. Bass, L. C. Sutherland, A. J. Zuckerwar, A. T. Blackstock, and D. M. Hester. "Atmospheric Absorption of Sound: Further Developments." *J. Acoust. Soc. Am.*, 97(1), 680–683, 1995.

[3] H. E. Bass, L. C. Sutherland, A. J. Zuckerwar, A. T. Blackstock, and D. M. Hester. "Erratum: Atmospheric Absorption of Sound: Further Developments." *J. Acoust. Soc. Am.*, 99(2), 1259–1259, 1996.

[4] L. Bertsch, W. Dobrzynski, and S. Guérin. "Tool Development for Low-Noise Aircraft Design." *J. Aircraft*, 47(2), 694–699, 2010.

[5] T. F. Brooks and W. M. Humphreys. "Flap Edge Aeroacoustic Measurements and Predictions." AIAA-2000-1975, 2000. Sixth AIAA/CEAS Aeroacoustics Conference, Lahaina, Hawaï, USA, June 12-14, 2000.

[6] L. Brusniak, J. R. Underbrink, and R. W. Stoker. "Acoustic Imaging of Aircraft Noise Sources using Large Aperture Phased Arrays." AIAA-2006-2715, 2006. Twelfth AIAA/CEAS Aeroacoustics Conference, Cambridge, Massachusetts, USA, May 8-10, 2006.

[7] W. Dobrzynski, L. C. Chow, P. Guion, and D. Shiells. "A European Study on Landing Gear Noise Sources." AIAA-2000-1971, 2000. Sixth AIAA/CEAS Aeroacoustics Conference, Lahaina, Hawaï, USA, June 12-14, 2000.

[8] W. Dobrzynski and M. Pott-Pollenske. "Slat Noise Source Studies for Farfield Noise Prediction." AIAA-2001-2158, 2001. Seventh AIAA/CEAS Aeroacoustics Conference and Exhibit, Maastricht, The Netherlands, May 28-30, 2001.

[9] G. Elias. "Source Localization with a Two-Dimensional Focused Array : Optimal Signal Processing for a Cross-Shaped Array." Inter-Noise, 1995.

[10] M. R. Fink. "Airframe Noise Prediction Method." Technical Report RD-77-29, FAA, 1977.

[11] V. Fleury and J. Bulté. "Extension of Deconvolution Algorithms for the Mapping of Moving Acoustic Sources." *J. Acoust. Soc. Am.*, 129(3), 1417–1428, 2011.

[12] S. Guérin, U. Michel, H. Siller, U. Finke, and G. Saueressig. "Airbus A319 Database from Dedicated Flyover Measurements to Investiagte Noise Abatement Procedures." AIAA-2005-2981, 2006. Eleventh AIAA/CEAS Aeroacoustics Conference, Monterey, California, USA, May 23-25, 2005.

[13] P. C. Hansen. "Rank-Deficient and Discrete Ill-Posed Problems: Numerical Aspects of Linear Inversion." SIAM, Philadelphia, 1998.

[14] M. S. Howe. "On the Generation of Side-Edge Flap Noise." *J. Sound and Vibration*, 61, 437–465, 1978.

[15] M. S. Howe. "A Review of the Theory of Trailing Edge Noise." *J. Sound and Vibration*, 80(4), 555–573, 1982.

[16] L. V. Lopes and C. L. Burley. "Design of the Next Generation Aircraft Noise Prediction Program: Annopp2." AIAA-2011-2854, 2011. Seventeenth AIAA/CEAS Aeroacoustics Conference, Portland, Oregon, USA, June 5-8, 2011.

[17] P. Malbéqui, Y. Rozenberg, and J. Bulté. "Aircraft Noise Modelling and Assessment in the iesta Program.", 2011. Inter-Noise, Osaka, Japan, Sept. 4-7, 2011.

[18] N. Molin and M. Roger. "The Use of Amiet's Methods in Predicting the Noise from 2d High-Lift Devices." AIAA-2000-2064, 2000. Sixth AIAA/CEAS Aeroacoustics Conference, Lahaina, Hawaï, USA, June 12-14, 2000.

[19] N. Molin, M. Roger, and S. Barré. "Prediction of Aircraft High-Lift Device Noise using Dedicated Analytical Models." AIAA-2003-3225, 2003. Ninth AIAA/CEAS Aeroacoustics Conference and Exhibit, Hilton Head, South Carolina, USA, May 12-14, 2003.

[20] J. A. Parker, R. V. Kenyon, and D. E. Troxel. "Comparison of Interpolation Methods for Image Resampling." *IEEE Trans. Med. Imag.*, MI-2(1), 31–39, 1983.

[21] M. Pott-Pollenske, W. Dobrzynski, S. Guérin, G. Saueressig, and U. Finke. "Airframe Noise Characteristics from Flyover Measurements and Prediction." AIAA-2006-2567, 2006. Twelfth AIAA/CEAS Aeroacoustics Conference (27th AIAA Aeroacoustics Conference), Cambridge, Massachusetts, USA, May 8-10, 2006.

[22] P. Sijtsma and R. Stoker. "Determination of Absolute Contributions of Aircraft Noise Components using Fly-Over Array Measurements." AIAA-2004-2958, 2004. Tenth AIAA/CEAS Aeroacoustics Conference, Manchester, United Kingdom, 2004.

[23] H. Siller and M. Drescher. "Investigation of Engine Tones in Flight." AIAA-2011-2946, 2011. Seventeenth AIAA/CEAS Aeroacoustics Conference (thirty-second AIAA Aeroacoustics Conference), Portland, Oregon, USA, June 5-8, 2011.